Publication IV

Ilkka Laakso. 2009. Assessment of the computational uncertainty of temperature rise and SAR in the eyes and brain under far-field exposure from 1 to 10 GHz. Physics in Medicine and Biology, volume 54, number 11, pages 3393-3404.

IOP PUBLISHING PHYSICS IN MEDICINE AND BIOLOGY

Phys. Med. Biol. **54** (2009) 3393–3404 doi:10.1088/0031-9155/54/11/008

Assessment of the computational uncertainty of temperature rise and SAR in the eyes and brain under far-field exposure from 1 to 10 GHz

Ilkka Laakso

Department of Radio Science and Engineering, Helsinki University of Technology, Otakaari 5 A, 02150 Espoo, Finland

E-mail: ilkka.laakso@tkk.fi

Received 6 March 2009, in final form 20 April 2009
Published 13 May 2009
Online at stacks.iop.org/PMB/54/3393

Abstract

This paper presents finite-difference time-domain (FDTD) calculations of specific absorption rate (SAR) values in the head under plane-wave exposure from 1 to 10 GHz using a resolution of 0.5 mm in adult male and female voxel models. Temperature rise due to the power absorption is calculated by the bioheat equation using a multigrid method solver. The computational accuracy is investigated by repeating the calculations with resolutions of 1 mm and 2 mm and comparing the results. Cubically averaged 10 g SAR in the eyes and brain and eye-averaged SAR are calculated and compared to the corresponding temperature rise as well as the recommended limits for exposure. The results suggest that 2 mm resolution should only be used for frequencies smaller than 2.5 GHz, and 1 mm resolution only under 5 GHz. Morphological differences in models seemed to be an important cause of variation: differences in results between the two different models were usually larger than the computational error due to the grid resolution, and larger than the difference between the results for open and closed eyes. Limiting the incident plane-wave power density to smaller than 100 W m^{-2} was sufficient for ensuring that the temperature rise in the eyes and brain were less than 1 °C in the whole frequency range.

(Some figures in this article are in colour only in the electronic version)

1. Introduction

Intense exposure to radio-frequency electromagnetic (EM) fields may cause heating of tissues with potentially harmful effects. Recommendations which limit the exposure have been issued by, for example, the International Commission on Non-Ionizing Radiation Protection (ICNIRP 1998) and the Institute of Electrical and Electronics Engineers (IEEE 2005). Temperature rise

in the eyes under exposure to EM fields have been studied computationally for several different scenarios, including far-field exposure (Bernardi *et al* 1998, Hirata *et al* 2000, Hirata *et al* 2002, Hirata *et al* 2007) as well as different near-field sources (Wainwright 2000, Hirata 2005, Buccella *et al* 2007, Wainwright 2007, Flyckt *et al* 2007). Temperature rise due to cellular phones has been studied several times and it has been concluded that significant temperature rises in the brain are very unlikely (Leeuwen *et al* 1999, Wang and Fujiwara 1999, Bernardi *et al* 2000, Gandhi *et al* 2001). Several studies have shown that spatially averaged SAR at basic restriction limits may lead to temperature rise larger than 1 °C, which has been the basis for the recommendations (Hirata *et al* 2007).

The majority of the studies have used a finite-difference time-domain (FDTD) method for solving the electromagnetic problem and bioheat equation for thermal modelling. There are various sources of uncertainty and variation in this kind of combined FDTD and temperature simulations. Usually, the temperature rises have been small so thermoregulatory response has been ignored which may have lead to overestimation. The temperature rises are affected by, for example, the heat transfer model of the eye and value of choroidal blood flow (Wainwright 2007, Buccella *et al* 2007). Several causes of variation, such as eye mass, choroidal blood flow, blood perfusion rate of the skin, were discussed in Hirata *et al* (2007). The vascularized heat transfer model has been used instead of the bioheat equation (Leeuwen *et al* 1999, Flyckt *et al* 2006, Flyckt *et al* 2007), and the bioheat equation has been shown to provide good approximation of the more sophisticated model for low temperature rises. Especially in the case of young children, some uncertainty may rise from the dielectric material parameters (Keshvari *et al* 2006, Peyman *et al* 2009). SAR values also depend on how they are actually calculated; because the description of SAR averaging in ICNIRP (1998) guidelines is somewhat vague, various different SAR averaging methods have been considered in several studies (Hirata *et al* 2006, Wainwright 2007, Flyckt *et al* 2007). If near-field exposure is studied, different positioning of sources in different FDTD codes may produce significant variation in SAR values (Beard *et al* 2006). One important source of variation is the morphological differences in models. This has been discussed in several studies which employed more than one human model, e.g. (Hirata *et al* 2007, Buccella *et al* 2007).

This study will focus on assessing how large is the uncertainty due to grid resolution of the computational model. Previously, Mason *et al* (2000) studied plane-wave exposure of visible human model up to 1.8 GHz. Altering voxel size from 3 mm^3 to 5 mm^3 had 'very little' influence on the whole-body SAR values. The effect of resolution on the whole-body SAR and the peak spatial averaged SAR in the visible human model were also discussed in Kühn *et al* (2009) for 835 MHz and 2140 MHz. In that study, the difference between 1 mm and 2 mm in the whole-body and spatial-peak SAR values was reported to be small. Effects of resolution have also been presented by Dimbylow and Bolch (2007), who studied the whole-body SAR in various child models up to 6 GHz. Their results suggested *inter alia* that 1 mm resolution should be used instead of 2 mm for frequencies higher than ∼1 GHz. SAR values tended to become smaller when lower resolution was employed. Uusitupa *et al* (2008) studied the whole-body SAR as well as the peak 10 g SAR at 900 MHz and 1800 MHz for 1.8 mm and 3.6 mm resolution whole-body model. According to their results, the effects of resolution are affected by the SAR computation method and how the materials are set up in the FDTD grid.

In this study, simulations of SAR and temperature rise in the human head under plane-wave exposure are performed. High 0.5 mm resolution adult male and female voxel models are employed which allows whole-head simulations for frequencies as high as 10 GHz. Cubically averaged 10 g SAR in the eyes and brain and eye-averaged SAR are calculated and compared with the corresponding temperature rise values and exposure guidelines. The computational accuracy is assessed by repeating the calculations with resolutions of 1 mm and 2 mm and

comparing the results. The simulations are performed for three plane-wave incident angles and for models with eyes opened or closed, which gives more data for comparison between the resolutions and allows assessment of what kind of effects opening or closing the eyes has on temperature rise and SAR. The uncertainty analysis of the resolution will be useful not only for thermal calculations in the head but also for other FDTD-SAR simulations.

2. Methods and models

2.1. Finite-difference time-domain method

The widely used finite-difference time-domain (FDTD) method (Taflove and Hagness 2005) was used to solve the absorbed electromagnetic power inside the head tissues. The employed in-house FDTD code has been implemented in Fortran using MPI (message passing interface) libraries for parallelization. The performance of the solver has been previously verified by measurements (Ilvonen *et al* 2008). In terminating the computational domain, eight-cell thick convolutional perfectly matched layer (CPML) boundary conditions (Roden and Gedney 2000) were used. The performance of PML for SAR calculations has been tested previously in Findlay and Dimbylow (2006), Laakso *et al* (2007), where the computational uncertainty due to the absorbing boundary conditions was found to be negligible in numerous different cases.

The performance of the FDTD method is subject to discretization errors depending on the ratio of cell resolution and wavelength λ (Taflove and Hagness 2005). To maintain sufficient accuracy, a rule-of-thumb value of $\lambda/10$ for the maximum applicable cell size has been commonly used for homogeneous media. Using a finer resolution provides better accuracy and allows simulation of higher frequencies, but also needs more computer resources. For example, halving the cell size increases memory requirements eight fold and doubles the number of required time steps, resulting in 16 fold increase in operation count. In this study, the largest simulations with a 0.5 mm head model took about 90 min using eight processing cores in a supercomputer at CSC (Finnish IT Center for Science).

2.2. Bioheat equation

The temperature rise due to the absorption of electromagnetic power is in this study solved by the bioheat equation (Pennes 1948). Assuming steady-state condition and ignoring thermoregulatory response similar to Wainwright (2000), the equation for the temperature rise ΔT is an elliptic equation of the form

$$\nabla \cdot (k \nabla \Delta T) - B \Delta T + S = 0 \tag{1}$$

with boundary condition

$$k \frac{\partial \Delta T}{\partial n} + H \Delta T = 0, \tag{2}$$

where k is the thermal conductivity, B is related to the blood perfusion rate, S is the electromagnetic power-loss density calculated by FDTD and H is the heat transfer coefficient from tissue to air. This thermal model is likely to cause overestimation of the temperature rise, because of steady-state condition and ignoring thermoregulatory response. The overestimation due to assuming steady-state condition may be assessed by considering that the temperature during the rise to the steady state is approximately $\Delta T[1 - \exp(-t/\tau)]$, where ΔT denotes the steady-state temperature rise and τ is the thermal time constant, which is typically about 6–8 min (Leeuwen *et al* 1999, Wang and Fujiwara 1999, Bernardi *et al* 2000).

Table 1. Approximations of maximum applicable frequencies for different cell sizes in various tissues determined by the '$\lambda/10$' rule of thumb. The vitreous humour tissue has the shortest wavelength in the entire head. The average wavelength over the whole head does not include internal air.

Tissue/cell size	2 mm	1 mm	0.5 mm
Vitreous humour	1.8 GHz	3.7 GHz	7.6 GHz
Muscle	2.1 GHz	4.2 GHz	9.0 GHz
Grey matter	2.1 GHz	4.4 GHz	9.7 GHz
Skin	2.4 GHz	5.0 GHz	10.9 GHz
White matter	2.5 GHz	5.2 GHz	11.6 GHz
Average λ over the whole head	3.2 GHz	6.8 GHz	15.5 GHz

The bioheat equation was discretized using the same rectangular grid which was used in the FDTD simulations, with the unknown temperature nodes positioned in the centre points of the cells. As discussed in Samaras *et al* (2006), use of such staircase grid produces overestimation of heat transfer from body to air for curved boundaries. To reduce this staircase error, a simplified version of the heat transfer correction by Neufeld *et al* (2007) was used in this study. In this simplified scheme, the heat transfer coefficient H in (2) for each voxel on the body-air boundary is scaled according to

$$H \approx \frac{H_0}{\sqrt{N}}, \tag{3}$$

where N is the number of neighbouring air voxels and H_0 is the original heat transfer coefficient. The original conformal scheme by Neufeld *et al* (2007) requires information of the normal vector of the non-staircased boundary at each boundary voxel. In the simplified scheme this direction of the normal vector is approximated locally from the number of neighbouring air voxels, e.g., if $N = 3$, the direction of the normal vector is on average likely to be $\frac{1}{\sqrt{3}}(\pm 1, \pm 1, \pm 1)$ which results in the heat transfer from the cell divided by $\sqrt{3}$. The main advantage of the simplified scheme is easier implementation, and that the scheme can also be used for models without information of the normal vector. Heat transfer to air is decreased, so this approach gives conservative values compared to the uncorrected scheme.

The discretized equation was solved using the geometric multigrid method (Briggs 1987) with the Gauss–Seidel iteration which radically reduced the required computation time compared to the plain Gauss–Seidel (or SOR) method. The thermal calculations needed much less computational resources than the FDTD simulations: with an ordinary desktop computer using one processing core, residual norm 10^{-10} could be attained in about 15 min for a 0.5 mm resolution head model.

2.3. Head models and material parameters

Two head models were employed in this study, namely the adult male and female models from the Virtual Family Project (Christ *et al* 2009). The models are originally whole-body CAD models, from which voxelized head models with resolutions of 2 mm, 1 mm and 0.5 mm have been produced. The CAD models are based on MRI images, differently to, e.g. the electrogeometrical CAD model used in Buccella *et al* (2007). Electrical properties of tissues for different frequencies were calculated using the data in Gabriel *et al* (1996). Calculating the wavelengths and applying the '$\lambda/10$' rule of thumb for some important tissues gives the approximate maximum frequencies for each resolution and tissue, shown in table 1.

Table 2. Thermal parameters and densities (ρ) of the main tissues.

Tissue	k (W (m °C)$^{-1}$)	B (W (m^3 °C)$^{-1}$)	ρ (kg m^{-3})
Bone marrow	0.22	32 000	1027
Brain grey matter	0.57	40 000	1039
Brain white matter	0.50	40 000	1043
Cartilage	0.47	9000	1100
Cerebrospinal fluid	0.62	0	1007
Eye cornea	0.58	0	1076
Eye lens	0.40	0	1090
Eye sclera/retina/choroid	0.58	80 000	1032
Eye vitreous/aqueous humour	0.60	0	1009
Fat	0.25	1700	916
Mucosa	0.43	9000	1050
Muscle	0.50	2700	1041
Nerve	0.46	40 000	1038
Skin	0.42	9100	1100
Skull	0.40	3400	1990

Thermal parameters of tissues were based on the values presented in Bernardi *et al* (2003). The parameters for main tissues are shown in table 2. The heat transfer coefficient H_0 from skin to air was 8 W (m^2 K)$^{-1}$ and the coefficient from cornea to air was 20 W (m^2 K)$^{-1}$, similar to, e.g. Hirata *et al* (2007) and Wainwright (2007).

In the original models, the eyes are closed. For this study, eyes were opened by removing the eyelids, so that the differences in absorbed power and temperature rise between open and closed eyes could be studied. The masses of the right and left eyes are 6.7 g and 6.8 g for the male model and 8.4 g and 8.7 g for the female model. The original models contain only the sclera tissue without retina and choroid, due to the insufficient resolution for representing each tissue separately. For the 0.5 mm resolution model, the thickness of the sclera is 1–1.5 mm. In this study, this original sclera tissue is considered as a composite tissue, which consists of sclera, retina and choroid. The blood perfusion of this composite tissue was chosen to be 80 000 W (m K)$^{-1}$, the same as the lower value used in Hirata *et al* (2007).

2.4. Exposure scenario

In this study, plane waves are used as the exposure source. Plane waves allow easier comparison between different resolutions than near-field sources, the construction and positioning of which for different resolutions might bring additional uncertainty. Also, plane wave is likely to produce a more evenly distributed power-loss density than near-field sources, so the resulting temperature rise for the same averaged SAR value might be higher with plane waves (Buccella *et al* 2007).

Three different incident directions are studied: from the front, from the front left, and from 'upfront' (from the front and from above), as illustrated in figure 1. Using multiple incident angles give more data for the comparison between computational resolutions. Power density of the incident plane wave is 100 W m^{-2}, and it is vertically polarized. The power density corresponds to maximum permissible exposure by IEEE (2005) for frequencies over 3 GHz for people in controlled environments. The corresponding reference level for occupational exposure by ICNIRP (1998) is more restrictive: for frequencies over 2 GHz the level is 50 Wm^{-2}. Under 3 GHz and 2 GHz, respectively, the limits decrease linearly.

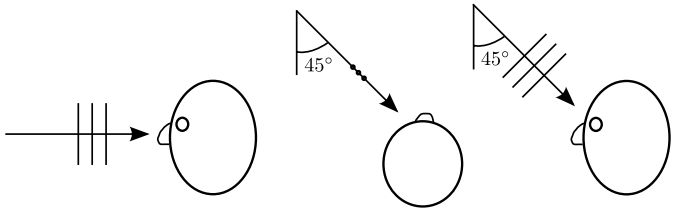

Figure 1. Incident angles of the plane wave: from the front, from the front left and from 'upfront'.

2.5. SAR averaging

ICNIRP (1998) guidelines use spatially averaged SAR for up to 10 GHz, but in the newer recommendations by IEEE (2005) spatially averaged SAR is only used as the basis for basic restriction limits for frequencies up to 3 GHz. The IEEE recommendations employ cubically averaged SAR, that is, the maximum SAR averaged over a cubical vo0lume of mass 10 g. In this study, the averaging cubes are determined as described in IEEE (2002), and their sizes are 'fine-tuned' as in Caputa *et al* (1999) so that their masses are exactly 10 g. By the method of Caputa *et al* (1999), each averaging cube consists of a core cube of full voxels and an outermost layer of fractions of voxels. Only the cubes whose centre point is located within the eye or brain are taken into account. Actually, IEEE (2005) would require that the maximum of cube-averaged SAR should be taken over the whole head. However, heat diffusion is only a few centimetres at most (Hirata *et al* 2006), so we only study the maximum 10 g SAR over the eye (or brain) which should be more closely related to the temperature rise in the eye than the maximum over the whole head. The ICNIRP limits do not specify the shape of the averaging volume, so the maximum cubically averaged SAR gives a lower bound for the ICNIRP-averaged SAR.

In addition to the cubically averaged SAR, also eye-averaged SAR was considered. It is calculated simply by dividing the total electromagnetic power loss in the eye by the eye mass. Previously, eye-averaged SAR has been observed to be a good measure for the maximum temperature rise in the eye for both near and far-field exposure setting, at least under 3 GHz (Hirata 2005, Wainwright 2007, Hirata *et al* 2007).

3. Results

The results of the simulations are presented in this section. All results are plotted as a function of frequency on a semi-logarithmic scale. Unless otherwise specified, only the results for the 0.5 mm resolution are shown.

3.1. SAR and temperature rise

Figures 2 and 3 show the averaged SAR values (cubically averaged and eye-averaged) in the left eye and the corresponding temperature rise in the left lens for front and front left incident angles, respectively. The upfront incident angle (not shown) gave smaller SAR values and temperature rises in the eyes than the other two. As seen in the figures, the maximum temperature rise in the lens always stayed under 1 °C when the power density of the incident plane wave was 100 Wm^{-2}. As can be seen in the figures, cubically averaged 10 g SAR seems to correlate well with the temperature rise in the lens. Eye-averaged SAR was quite

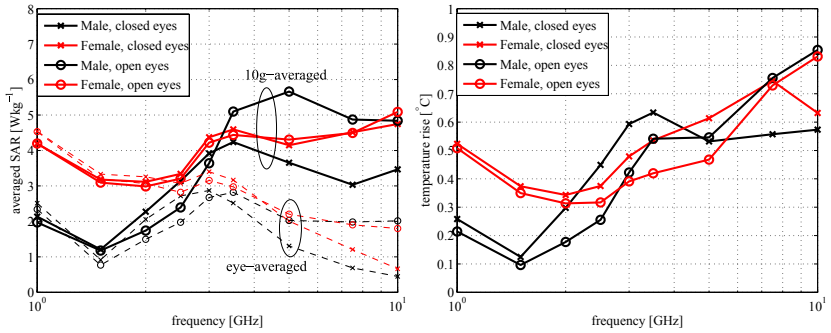

Figure 2. Averaged SAR (left) and the corresponding temperature rise (right) in the left lens for the plane-wave incident from the front. The thin dashed curves in the left figure mean eye-averaged SAR, and the corresponding thick solid curves are for the 10 g cubically averaged SAR.

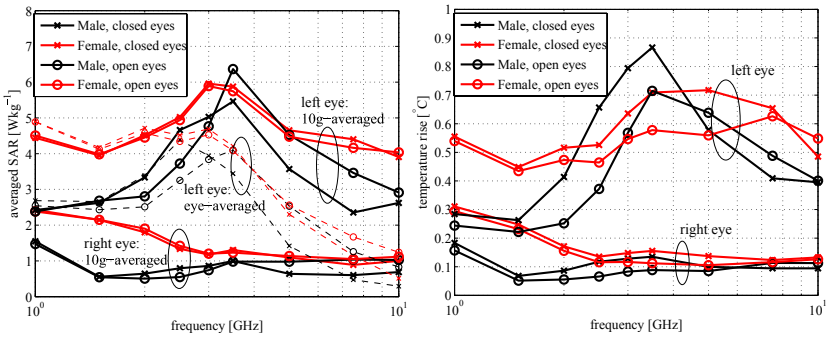

Figure 3. Averaged SAR (left) and the corresponding temperature rise (right) in the lens for the plane-wave incident from the front left. The thin dashed curves in the left figure mean eye-averaged SAR of the left eye. The thick solid curves are the 10 g cubically averaged SAR in the left eye (upper four curves) and in the right eye (lower four).

similar to 10 g averaged SAR at low frequencies but gave significantly lower values at higher frequencies. The maximum temperature rise over the whole eye (not shown) was always less than 0.2 °C (0.05 °C on average) higher than the corresponding maximum temperature rise in the lens. The use of staircase correction, as described in section 2.2 only had a minor effect on the temperature rise, giving 2–11% higher temperatures in the lens than without correction. The difference was slightly larger for open eyes and increased with frequency.

The peak 10 g averaged SAR and peak temperature rise in the brain are shown in figure 4. The figure shows the results for all three incident angles and both models (open or closed eyes did not affect the results). It seems that both SAR and temperature rise generally are slightly smaller than the corresponding values in the eyes. Similar to the case of the eyes, the difference between the results of male and female models is large. SAR values seem to decrease at high frequencies, which can be attributed to the decreasing penetration depth and the fact that only the averaging cubes whose centre points were located in the brain were considered.

Figure 5 shows the ratio of the peak 10 g cubically averaged SAR and the maximum temperature rise in the lens and in the brain. In the eyes, the ratio was quite similar for all incident angles and both eyes, so for each frequency and model, the shown values are averages

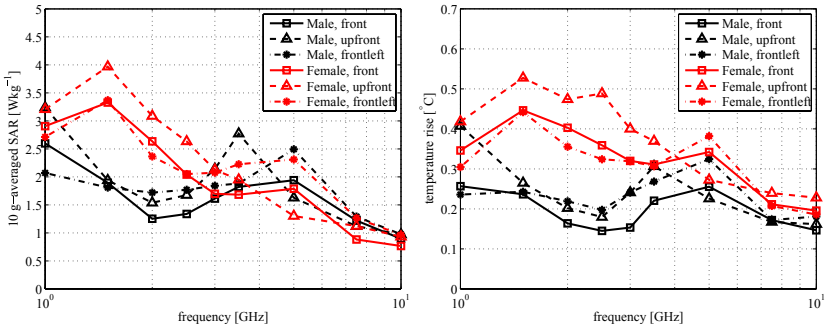

Figure 4. Maximum cubically averaged SAR (left) and the corresponding maximum temperature rise (right) in the brain for various incident angles.

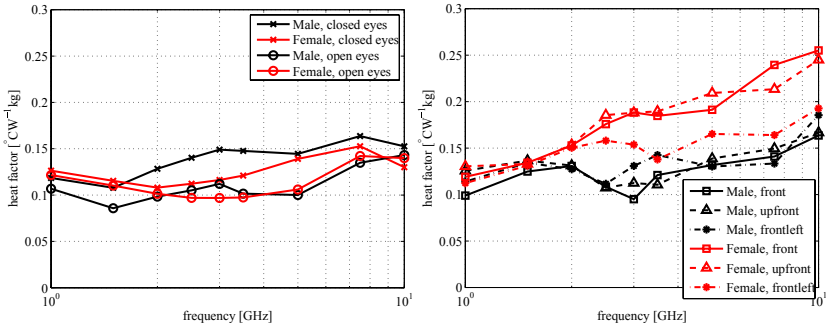

Figure 5. Left figure shows the ratio of maximum temperature rise in the lens and maximum cubically averaged 10 g SAR in the eye. For each frequency and model, the shown values are averages over the three incident angles and left and right eyes. The similar ratio for the brain is shown in the right figure for various incident angles.

over six cases: the three incident angles and left and right eyes. The ratio in the lens seems to be typically in the range 0.1–0.15, which is in line with previous studies (Hirata *et al* 2007). If the ratio were calculated with respect to the eye-averaged SAR instead of 10 g SAR, it would increase rapidly at frequencies higher than 3 GHz, as was also observed in Hirata *et al* (2007). In the brain, the ratio seems to grow slightly at high frequencies, which is due to the fact that SAR values decrease faster than the temperature rise. The female model gives significantly higher ratios than the male model for front and upfront incident angles, which might be related to the different anatomical details near the location of the maximum SAR and temperature rise.

3.2. Effects of resolution

To study the effect of grid resolution, various averaged SAR key values and temperature rise values calculated with lower resolutions were compared with the 0.5 mm resolution results, which were considered the most accurate. For each frequency, a total of 24 (for brain: 6) cases, i.e. both models, all three incident angles, left and right eyes, as well as open and closed eyes, were considered. For each case, the ratio of 1 mm or 2 mm result value and the corresponding 0.5 mm result was calculated, and the total range of variation for each frequency

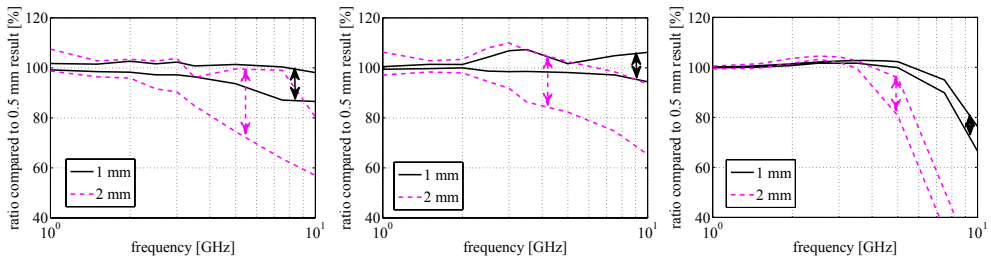

Figure 6. Range of variation of 2 mm and 1 mm results compared to 0.5 mm results for various SAR values, 100% = 0.5 mm result. Maximum 10 g averaged SAR in the eyes (left), in the brain (middle) and SAR averaged over the whole brain (right).

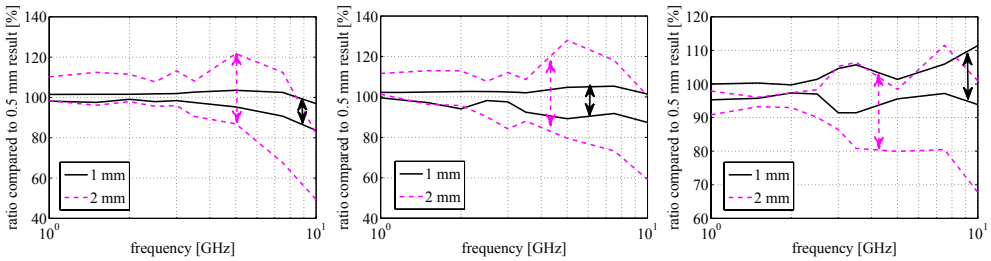

Figure 7. Range of variation of 2 mm and 1 mm results compared to 0.5 mm results, 100% = 0.5 mm result. Maximum temperature rise in the lens (left), in the whole eye (middle) and in the brain (right).

was determined. Figures 6 and 7 show the range of variation for some key SAR values and temperature rise values, respectively. It seems that too low resolution will typically, but not always, result in error which tends to cause underestimation of the SAR values, which is in agreement with previously reported results (Dimbylow and Bolch 2007). This underestimation seems to be more apparent for values which are averaged over large volumes, such as the whole brain.

4. Discussion

Based on the results it is possible to derive empirical rules of thumb for sufficient resolution for the calculation of averaged SAR values and temperature rise. By figures 6 and 7, it seems that 2 mm resolution might be sufficient for frequencies smaller than 2.5–3 GHz, with typical variation from 0.5 mm results less than 10%. The range of variation is smaller for the 1 mm resolution, and the maximum frequency seems to be 5 GHz, after which the results start to diverge from the 0.5 mm results. Comparison with table 1 shows that these maximum frequencies approximately match the '$\lambda/10$' rule of thumb for the ratio of cell size and the wavelength for, e.g. the skin or brain tissues. It seems that if this rule is satisfied, uncertainty in SAR and temperature values due to resolution is typically smaller than ± 10 %, which is not negligible but may be small compared to the other possible sources of uncertainty such as morphological differences in models.

In all the studied cases, incident power density 100 W m^{-2} ensured that the temperature rise in the lens was less than 1 °C. Likewise, cubically averaged SAR values in the eye were always smaller than 7 W kg^{-1}. In the brain the temperature rise was always less than 0.6 °C

and the peak 10 g SAR stayed below 4 W kg^{-1}. Consequently, reference levels (ICNIRP 1998) and maximum permissible exposure levels (IEEE 2005) seem to be conservative in the studied cases, at least when only eyes and brain are considered. IEEE does not use SAR for frequencies higher than 3 GHz because of low penetration depth of microwaves at high frequencies. Still, cubically averaged 10 g SAR (IEEE 2002) seems to give good correlation with the temperature rise. In the eyes, the ratio of 10 g cubically averaged SAR and the temperature rise stayed relatively constant between 0.10 and 0.15 in the whole frequency range 1–10 GHz. In the brain, the ratio was somewhat similar in magnitude, but it increased somewhat at the higher frequencies, where the skin depth of the microwaves becomes smaller. It seems that maximum 10 g SAR of 10 W kg^{-1} in the eyes or brain could cause temperature rises larger than 1 °C, but it should be noted that the calculated values are likely to be overestimation of the real temperature rise.

Cubically averaged 10 g SAR in the eyes seems to be more useful than eye-averaged SAR in predicting the temperature rise in the lens. Both SAR values are quite similar in magnitude at frequencies lower than 3 GHz. But unlike cubically averaged 10 g SAR in the eyes, eye-averaged SAR decreases with frequency above 3 GHz as it does not take into account the power absorption in the surrounding tissues near the front of the eye. However the maximum temperature rise in the lens does not necessarily decrease. Consequently, eye-averaged SAR does not seem to be a good measure for temperature rise for frequencies larger than 3 GHz, which was also observed in Hirata *et al* (2007).

The two studied models are insufficient for making detailed conclusions on the effects of morphological variation on the results, but it seems that the power absorption in the eyes depends heavily on the anatomical details of the models. In particular, differences between male and female models were larger than the effect of open or closed eyes, especially in the lower end of the frequency range. Differences in results between the models were already large in the SAR distributions and did not seem to become larger after the thermal calculation was applied (figures 2 and 3), so it seems that morphological differences might not be as important for thermal calculations as they are for SAR calculations. In this case, with the possible thermoregulatory response ignored, closed eyes typically gave slightly higher temperature rise for the same peak 10 g SAR than open eyes, because heat diffusion into air was smaller due to the insulating eyelids. If the blood perfusion rate of the skin would be increased from the used value of 9100 W $(m^3\ °C)^{-1}$, the difference would be likely to become smaller.

5. Conclusion

Anatomically realistic male and female human models were exposed to plane waves incident from three directions. SAR and temperature rise in the eyes and brain were studied in the frequency range from 1 to 10 GHz. The calculations were performed using 0.5 mm, 1 mm and 2 mm resolutions, employing the FDTD method for the electromagnetic problem and the bioheat equation with the geometric multigrid solver for the thermal problem.

The results suggest that 2 mm resolution should only be used for frequencies smaller than 2.5 GHz, and 1 mm resolution only under 5 GHz. Under these frequencies, the variation in 10 g SAR values from the results of 0.5 mm resolution was typically smaller than ± 10%. Morphological differences in models seemed to be an important cause for variation: differences in results between the two different models were usually larger than the computational error due to the grid resolution, and larger than the difference between the results for open and closed eyes. The reference levels by ICNIRP and maximum permissible exposure limits by IEEE seemed to be conservative in the sense that at the reference levels the temperature rise in the eyes and brain was always less than 1 °C. On the other hand, the limits for cubically averaged

10 g SAR might not be as conservative because SAR of 10 W kg^{-1} in the eyes or in the brain could cause temperature rises larger than 1 °C, which might however be overestimation because of approximations in the thermal model.

Acknowledgments

Financial support received from GETA (Graduate School in Electronics, Telecommunication and Automation) is acknowledged. Computational resources of CSC (Finnish IT Center for Science) were utilized in this study.

References

Beard B B *et al* 2006 Comparisons of computed mobile phone induced SAR in the SAM phantom to that in anatomically correct models of the human head *IEEE Trans. Electromagn. Compat.* **48** 397–407

Bernardi P, Cavagnaro M, Pisa S and Piuzzi E 1998 SAR distribution and temperature increase in an anatomical model of the human eye exposed to the field radiated by the user antenna in a wireless LAN *IEEE Trans. Microw. Theory Tech.* **46** 2074–82

Bernardi P, Cavagnaro M, Pisa S and Piuzzi E 2000 Specific absorption rate and temperature increases in the head of a cellular-phone user *IEEE Trans. Microw. Theory Tech.* **48** 1118–26

Bernardi P, Cavagnaro M, Pisa S and Piuzzi E 2003 Specific absorption rate and temperature elevation in a subject exposed in the far-field of radio-frequency sources operating in the 10–900 MHz range *IEEE Trans. Biomed. Eng.* **50** 295–304

Briggs W L 1987 *Multigrid Tutorial* (Philadelphia, PA: SIAM)

Buccella C, De Santis V and Feliziani M 2007 Prediction of temperature increase in human eyes due to RF sources *IEEE Trans. Electromagn. Compat.* **49** 825–33

Caputa K, Okoniewski M and Stuchly M A 1999 An algorithm for computations of the power deposition in human tissue *IEEE Antennas Propag. Mag.* **41** 102–7

Christ A *et al* 2009 The virtual family—development of anatomical CAD models of two adults and two children for dosimetric simulations, in preparation

Dimbylow P and Bolch W 2007 Whole-body-averaged SAR from 50 MHz to 4 GHz in the University of Florida child voxel phantoms *Phys. Med. Biol.* **52** 6639–49

Findlay R P and Dimbylow P J 2006 Variations in calculated SAR with distance to the perfectly matched layer boundary for a human voxel model *Phys. Med. Biol.* **51** N411–5

Flyckt V M M, Raaymakers B W, Kroeze H and Lagendijk J J W 2007 Calculation of SAR and temperature rise in a high-resolution vascularized model of the human eye and orbit when exposed to a dipole antenna at 900, 1500 and 1800 MHz *Phys. Med. Biol.* **52** 2691–701

Flyckt V M M, Raaymakers B W and Lagendijk J J W 2006 Modelling the impact of blood flow on the temperature distribution in the human eye and the orbit: fixed heat transfer coefficients versus the Pennes bioheat model versus discrete blood vessels *Phys. Med. Biol.* **51** 5007–21

Gabriel S, Lau R W and Gabriel C 1996 The dielectric properties of biological tissues: III. Parametric models for the dielectric spectrum of tissues *Phys. Med. Biol.* **41** 2271–93

Gandhi O P, Kang G, Wu D and Lazzi G 2001 Currents induced in anatomic models of the human for uniform and nonuniform power frequency magnetic fields *Bioelectromagnetics* **22** 112–21

Hirata A 2005 Temperature increase in human eyes due to near-field and far-field exposures at 900 MHz, 1.5 GHz, and 1.9 GHz *IEEE Trans. Electromagn. Compat.* **47** 68–76

Hirata A, Fujimoto M, Asano T, Wang J, Fujiwara O and Shiozawa T 2006 Correlation between maximum temperature increase and peak SAR with different average schemes and masses *IEEE Trans. Electromagn. Compat.* **48** 569–78

Hirata A, Matsuyama S and Shiozawa T 2000 Temperature rises in the human eye exposed to EM waves in the frequency range 0.6-6 GHz *IEEE Trans. Electromagn. Compat.* **42** 386–93

Hirata A, Watanabe S, Fujiwara O, Kojima M, Sasaki K and Shiozawa T 2007 Temperature elevation in the eye of anatomically based human head models for plane-wave exposures *Phys. Med. Biol.* **52** 6389–99

Hirata A, Watanabe H and Shiozawa T 2002 SAR and temperature increase in the human eye induced by obliquely incident plane waves *IEEE Trans. Electromagn. Compat.* **44** 592–4

ICNIRP 1998 Guidelines for limiting exposure to time-varying electric, magnetic and electromagnetic fields (up to 300 GHz) *Health Phys.* **74** 492–522

IEEE 2002 *IEEE Recommended Practice for Measurements and Computations of Radio Frequency Electromagnetic Fields With Respect to Human Exposure to Such Fields, 100 kHz-300 GHz, C95.3-2002* (New York: IEEE)

IEEE 2005 *IEEE Standard for Safety Levels with Respect to Human Exposure to Radio Frequency Electromagnetic Fields, 3 kHz to 300 GHz, C95.1-2005* (New York: IEEE)

Ilvonen S, Toivonen T, Toivo T, Uusitupa T and Laakso I 2008 Numerical specific absorption rate analysis and measurement of a small indoor base station antenna *Microw. Opt. Techn. Lett.* **50** 2516–21

Keshvari J, Keshvari R and Lang S 2006 The effect of increase in dielectric values on specific absorption rate (SAR) in eye and head tissues following 900, 1800 and 2450 MHz radio frequency (RF) exposure *Phys. Med. Biol.* **51** 1463–77

Kühn S, Jennings W, Christ A and Kuster N 2009 Assessment of induced radio-frequency electromagnetic fields in various anatomical human body models. *Phys. Med. Biol.* **54** 875–90

Laakso I, Ilvonen S and Uusitupa T 2007 Performance of convolutional PML absorbing boundary conditions in finite-difference time-domain SAR calculations *Phys. Med. Biol.* **52** 7183–92

Leeuwen G M V, Lagendijk J J, Leersum B J V, Zwamborn A P, Hornsleth S N and Kotte A N 1999 Calculation of change in brain temperatures due to exposure to a mobile phone *Phys. Med. Biol.* **44** 2367–79

Mason P A, Hurt W D, Walters T J, D'Andrea J A, Gajsek P, Ryan K L, Nelson D A, Smith K I and Ziriax J M 2000 Effects of frequency, permittivity, and voxel size on predicted specific absorption rate values in biological tissue during electromagnetic-field exposure *IEEE Trans. Microw. Theory Tech.* **48** 2050–8

Neufeld E, Chavannes N, Samaras T and Kuster N 2007 Novel conformal technique to reduce staircasing artifacts at material boundaries for FDTD modeling of the bioheat equation *Phys. Med. Biol.* **52** 4371–81

Pennes H H 1948 Analysis of tissue and arterial blood temperature in the resting human forearm *J. Appl. Physiol.* **1** 93–122

Peyman A, Gabriel C, Grant E H, Vermeeren G and Martens L 2009 Variation of the dielectric properties of tissues with age: the effect on the values of SAR in children when exposed to walkie-talkie devices *Phys. Med. Biol.* **54** 227–41

Roden J A and Gedney S D 2000 Convolution PML (CPML): an efficient FDTD implementation of the CFS-PML for arbitrary media *Microw. Opt. Technol. Lett.* **27** 334–9

Samaras T, Christ A and Kuster N 2006 Effects of geometry discretization aspects on the numerical solution of the bioheat transfer equation with the FDTD technique *Phys. Med. Biol.* **51** N221–9

Taflove A and Hagness S C 2005 *Computational Electrodynamics: The Finite-Difference Time-Domain Method* 3rd edn (Boston, MA: Artech House)

Uusitupa T M, Ilvonen S A, Laakso I M and Nikoskinen K I 2008 The effect of finite-difference time-domain resolution and power-loss computation method on SAR values in plane-wave exposure of Zubal phantom *Phys. Med. Biol.* **53** 445–52

Wainwright P 2000 Thermal effects of radiation from cellular telephones *Phys. Med. Biol.* **45** 2363–72

Wainwright P R 2007 Computational modelling of temperature rises in the eye in the near field of radiofrequency sources at 380, 900 and 1800 MHz *Phys. Med. Biol.* **52** 3335–50

Wang J and Fujiwara O 1999 FDTD computation of temperature rise in the human head for portable telephones *IEEE Trans. Microw. Theory Tech.* **47** 1528–34